AO10 From the Sahara to Europe: Tracing the Rising Frequency of 3D Dust Transport Events

Candidate Name: Grace Choi
Candidate Number: 1074195
Supervisors: Dr. B. Swain and Prof. Roy G. Grainger

Abstract

Saharan dust transport to Europe has well-documented consequences on air quality and human health, and isolating the mineral dust signal from other aerosols can determine whether transport events are meaningfully evolving. Research has predominantly focussed on transport events in a limited selection of months rather than annual patterns. The purpose of this report is to investigate the year-round transport pathways of Saharan dust to Europe and the changes in dust event characteristics (intensity, duration, and frequency). For this purpose, Dust Extinction Aerosol Optical Depth data from reanalysis datasets was used to build a catalogue of dust events from 1980–2025 using threshold-based anomaly detection. Results indicate that dust signals remain persistent despite clean-air policies, with spring and summer being the peak seasons for transport towards Europe. Evolution of dust events depends upon the selected sample groups; events in the last five years are significantly more intense, particularly in February, and events in the last twenty years are significantly longer. A meaningful shift in the total aerosol composition driven by reduced anthropogenic emissions and increased dust transport could motivate further research into European climate projections due to the potential impact on regional warming. Climate-related public health planning could also require closer attention to dust event tracking to mitigate prolonged exposure to particulate matter. This is given a recent emergence of intense events at the end of winter.

1 Introduction

The transport of dust from the Sahara to Europe is a phenomenon that can often be identified by red or golden skies around sunrise and sunset resulting from elevated dust levels, and noticeable dust depositions. Studies note a recent increase in dust intrusions focussing on the Mediterranean, with a series of unusually strong dust events occurring between February–March 2020–2022. PM_{10} concentrations (referring to particulate matter with diameter $\leq 10\ \mu$m) well exceeded the healthy 24–hr average limit of 50 μg/m^3 [1].

Studying patterns of dust transport events is important as events have significant impacts on health and the economy. Elevated dust concentrations can reduce air quality and exacerbate respiratory conditions [2]. High dust loading during these events can also cause poor visibility, disrupting public transport systems and energy generation [3]. Global recognition of the risks surrounding sand and dust storms (SDS) is demonstrated by initiatives from the United Nations (UN), such as the recent launch of the UN Decade on Combating SDS (2025–2034) [4] and the UN Coalition on Combating SDS, bringing together a range of agencies to reduce SDS impacts on health, the economy, and the environment [5].

This report has three aims.

Firstly, the report aims to investigate the 45-year evolution (1980–2025) of trends in monthly Dust Extinction Aerosol Optical Depth (DOD) in relation to monthly Total Extinction Aerosol Optical Depth (AOD). Extinction Aerosol Optical Depth is a dimensionless measure of the extinction of incoming solar radiation caused jointly by scattering and absorption by all aerosols. DOD is the share of AOD attributed to mineral dust. Investigating DOD and AOD in parallel evaluates the changes in the balance between anthropogenic emissions and dust loading. By isolating reductions in AOD due to clean-air policies, this report explores the efficacy of emissions regulations and the effect on DOD levels. The report further investigates the transport pathways of dust events. This is achieved by tracing the vertical lifting and latitudinal movement of DOD signals seasonally, identifying a dust plume through 3D analysis, and using dust column mass flux vectors on a coordinate grid to track 2D sources and propagation of dust.

Secondly, the report aims to address a gap in year-round European dust event analysis by adopting existing threshold-based identification and categorisation methodologies. The report is interested in whether there has been a change in the frequency, duration, or intensity of such events over 1980–2025. An understanding of any shifts in the characteristics of dust events could inform future mitigation or adaptation strategies.

Thirdly, the report aims to investigate the relationship between total aerosol loading and climate variables to provide further insight into the drivers of changes in regional near-surface air temperature and precipitation.

The structure of this report is as follows. Section 2 details the datasets, software, and methods used for dust event identification and categorisation, and the effects of aerosol forcing on climate variables. Section 3 discusses the results of the AOD and DOD trend analysis, dust event characteristics, and impacts of aerosol forcing. Section 4 presents the conclusions.

2 Methods

2.1 Dust Event Identification & Categorisation

Datasets from the Modern-Era Retrospective Analysis for Research and Applications, Version 2 (MERRA-2) were utilised in this report for the identification and categorisation of dust events. Climate Data Operators (CDOs) were used for data processing.

MERRA-2 corrects predictions from the Goddard Earth Observing System Version 5.12.4 (GEOS-5.12.4) with satellite-based data, including from the Advanced Very High-Resolution Radiometer (AVHRR), Moderate Resolution Imaging Spectroradiometer (MODIS), and the Multi-angle Imaging Spectroradiometer (MISR), and ground-based AERONET observations. GEOS-5.12.4 consists of the GEOS-5 atmospheric model and the Gridpoint Statistical Interpolation (GSI) analysis scheme. Aerosol analysis further uses the GEOS-5 Goddard Aerosol Assimilation System (GAAS) with the Goddard Chemistry, Aerosol, Radiation, and Transport (GOCART) model. Datasets have a spatial resolution of 0.5° latitude by 0.625° longitude, and temporal resolution of one hour. MERRA2 provided data for DOD (550nm), AOD (550nm), dust column u-wind mass flux (DUFLUXU) and dust column v-wind mass (DUFLUXV) [6, 7].

CDOs were used to divide the data into three regions: (1) Europe (10°W, 30°E, 46°N, 60°N), (2) the Mediterranean (10°W, 30°E, 30°N, 46°N), and (3) the Sahara (20°W, 30°E, 15°N, 30°N). Comparisons of AOD and DOD regional averages were made over these three regions between two time periods: (1) 1980–1999, and (2) 2000–2025. These time divisions were chosen to provide a roughly equal split of available MERRA-2 data, and to investigate whether the observed decrease in AOD post-2000 was accompanied by changes in dust aerosol levels or event characteristics.

Dust event identification was conducted using a threshold-based anomaly detection for Europe, using a climatological mean ($\mathrm{DOD_{clim}}$) and standard deviation to define thresholds for dust categories as seen in Table 1. The criteria were based on a methodology proposed by Gkikas, et al. [8] and used by Cuevas-Agulló, et al. [9]. In these papers, the methodology uses AOD to determine statistical thresholds. This report used DOD to better capture instances of elevated dust loading rather than overall aerosol loading.

Category	Criteria
Moderate	$\mathrm{DOD_{clim}} + \sigma < \mathrm{DOD_{avg}} \leq \mathrm{DOD_{clim}} + 2\sigma$
Strong	$\mathrm{DOD_{clim}} + 2\sigma < \mathrm{DOD_{avg}} \leq \mathrm{DOD_{clim}} + 4\sigma$
Extreme	$\mathrm{DOD_{avg}} > \mathrm{DOD_{clim}} + 4\sigma$

Table 1: Climatological mean ($\mathrm{DOD_{clim}}$) and standard deviation (σ) criteria for dust categories over Europe and the Mediterranean using MERRA-2 DOD for 1980–2025.

$\mathrm{DOD_{clim}}$ was calculated on a seasonal basis by Equation 1, where s denotes season, N_s is the total number of days in s over 1980–2025, and $\overline{\mathrm{DOD}}(d, Y)$ is the spatially averaged $\mathrm{DOD_{daily}}$ over Europe on day d of year Y. This yields four values of $\mathrm{DOD_{clim}}$ corresponding to the four seasons: winter (DJF), spring (MAM), summer (JJA), and autumn (SON).

$$\mathrm{DOD_{clim}}(s) = \frac{1}{N_s} \sum_{\substack{Y=1980 \\ d \in s}}^{2025} \overline{\mathrm{DOD}}(d, Y) \qquad (1)$$

The standard deviation $\sigma(s)$ is calculated by Equation 2.

$$\sigma(s) = \sqrt{\frac{1}{N_s - 1} \sum_{Y, d \in s} \left(\overline{\mathrm{DOD}} - \mathrm{DOD_{clim}}\right)^2} \qquad (2)$$

To identify dust events, each day from 1980–2025 is first sorted into one of the above dust categories. For dust days, $\mathrm{DOD_{avg}}$ is taken as the daily spatial average $\overline{\mathrm{DOD}}(d)$. The occurrence of a dust event is qualified by a minimum of three consecutive dust days in any category. The start of a dust event is identified with the occurrence of a dust day, when $\overline{\mathrm{DOD}}(d) > \mathrm{DOD_{clim}} + \sigma$. If the following two days also qualify as dust days, a dust event is recorded and continues until the absence of a dust day is recorded when $\overline{\mathrm{DOD}}(d) \leq \mathrm{DOD_{clim}} + \sigma$. The intensity of the event $\mathrm{DOD_{avg}}$ is calculated by averaging $\overline{\mathrm{DOD}}(d)$ over the duration of the event. $\mathrm{DOD_{avg}}$ is then used to sort the event into one of the categories:

moderate, strong, or extreme. It is worth noting that this approach identifies a fixed proportion of days in the distribution as dusty relative to DOD_{clim}, rather than applying fixed physical thresholds. This results in the detection of relative anomalies rather than capturing all physically significant dust events.

The values for the dust category thresholds computed from $DOD_{clim}(s)$ and $\sigma(s)$ vary by season in Table 2. Spring displays the highest thresholds, consistent with literature identifying the seasonality of dust transport from the Sahara being especially prevalent in March.

Season	Moderate	Strong	Extreme
Winter (DJF)	0.022	0.034	0.058
Spring (MAM)	0.060	0.085	0.135
Summer (JJA)	0.035	0.049	0.077
Autumn (SON)	0.028	0.041	0.067

Table 2: Seasonal climatological lower thresholds for Europe based on $\overline{DOD}(d)$ (1980–2025). Moderate, strong, and extreme lower thresholds are defined as $\mu+\sigma$, $\mu+2\sigma$, and $\mu+4\sigma$ respectively.

A range of methods for specifying DOD_{clim} and σ was considered. Having an annual climatological mean was deemed unsuitable as there were clear seasonal trends of high dust loading in spring and summer months from 1980–2025. An alternative methodology used $\overline{DOD}_{monthly}$ (spatially averaged monthly mean DOD) in place of $\overline{DOD}(d)$ to compute climatological means and standard deviations for each month, resulting in 12 values for DOD_{clim} and σ. This was intended to capture true outlier events on a monthly basis, with April and May showing the highest thresholds for classification as a dust event (See Figure A1). However, using $\overline{DOD}_{monthly}$ had the effect of screening out daily variations in dust loading when calculating DOD_{clim} and σ. Whilst DOD_{clim} remained similar between methodologies, the σ of $\overline{DOD}_{monthly}$ values was lower, resulting in a narrowed threshold range between moderate, strong, and extreme events. This had the consequence of identifying an excessive number of extreme dust events compared to existing literature in spring, and events with very low DOD being classified as extreme in winter. Therefore, seasonal thresholds were found to be the preferred method.

In order to investigate the 3D transport mechanisms of dust transport from the Sahara, monthly mean AODDust (DOD at 500nm) was simulated using a 2003–2012 run of the GEOS-Chem 3D chemical transport model [10]. GEOS-Chem models atmospheric composition driven by assimilated meteorological observations from GEOS-5.12.4. The resolution of the simulation was 4° latitude by 5° longitude with a hybrid 72-level vertical grid, using a spatial coordinate near the ground surface and transitioning to a pressure-based coordinate with increasing altitude. A 2D coordinate grid of MERRA-2 DUFLUXU and DUFLUXV monthly means was also used to investigate dust transport pathways, showing the east-west and north-south components of mass flux of dust in a vertical column.

2.2 Dust Event Characteristics

Three characteristics of dust events were analysed: frequency (number of events per month), intensity (DOD_{avg}), and duration (days in event). The time span of the study (1980–2025) was divided into two periods. The first division compared 1980–1999 with 2000–2025, and the second division compared 1980–2019 with 2020–2025 in line with recent literature noting an influx of dust events from 2020–2022.

Gaussian distributions were fitted to the three characteristics to analyse changes in distribution between the two periods for Europe. Log-normal fitting was also deemed appropriate for duration and intensity data due to the right-skewed distribution of event duration (skewness=2.686) and DOD_{avg} (skewness=1.415) (See Appendix C). Log-normal fitting was not used for frequency due to the data's discreteness. A two-tailed independent t-test was applied to both raw and log-transformed data, with significance level set as $p < 0.05$ for all three characteristics.

One-tailed Mann-Whitney U tests were applied on a monthly basis to test the hypotheses that there are increases in frequency, intensity, or duration of dust events between the two periods for a specific month. This test was deemed appropriate due to the skewed nature of the data and smaller sample sizes. Significance level was set as $p < 0.05$.

2.3 AERONET Comparison

Data from ground-based observations was taken from the Aerosol Robotic Network (AERONET). AERONET uses sun photometer measurements to calculate AOD for variety of wavelengths λ and the Angstrom exponent α, which are related by Equation 3.

$$\alpha = -\frac{d \ln \mathrm{AOD}}{d \ln \lambda} \qquad (3)$$

Level 2.0 data for the daily averages of AOD

(500nm) and α (440-870nm) was downloaded from AERONET Version 3 Direct Sun for all sites based on data availability [11]. These were then filtered to retain 121 sites in Europe within the coordinate bounds (Figure B1). AERONET AOD (500nm) from these sites was compared with MERRA-2 AOD (550nm) over Europe, computing the Pearson correlation coefficient r, bias, and the Root Mean Square Error (RMSE) to assess agreement with reanalysis aerosol data.

To evaluate the consistency of the dust event identification and categorisation methodology with ground-based observations, α (440-870nm) was plotted against AERONET AOD (500nm) to investigate the aerosol size distribution during and outside dust events. Periods dominated by anthropogenic aerosols (e.g. biomass burning or pollution) are expected to show high α. This is because fine mode aerosols of radius 0.1-1 μm result in selective scattering for different λ values. This effect is less pronounced for larger particles and so, during moderate, strong or extreme dust events, lower α and high AOD are expected as dust is a coarse mode aerosol with radius 1-10 μm, with α expected to be lower for more intense events.

2.4 Climate Variables

Data from the Coupled Model Intercomparison Project Phase 6 (CMIP6) informed the investigation of the effects of historical and future total aerosol forcing on near-surface air temperature (`tas`) and mean precipitation flux (`pr`). CMIP6 is the latest phase in the project, which consists of an international network of over 50 climate modelling groups working to simulate changes in Earth's climate. Specifically, the report used the Detection and Attribution Model Intercomparison Project (DAMIP), which isolates the effect of total aerosol forcing on `tas` and `pr` whilst holding other factors, such as greenhouse gas emissions, fixed.

Annual mean data for `tas` from 1850 to 2100 inclusive was considered from five models based on data availability: the Canadian Earth System Model version 5 (CanESM5), the Hadley Centre Global Environment Model version 3 (HadGEM3), the Institut Pierre-Simon Laplace CM6A-LR (IPSL-CM6A), the Model for Interdisciplinary Research on Climate version 6 (MIROC6), and the Norwegian Earth System Model (NorESM2-LM). Historical runs using aerosol-only forcing spanned 1850–2020 with data from CanESM5, HadGEM3, IPSL-CM6A, and MIROC6.

The projections for total aerosol forcing effects from 2021–2100 ran under the Shared Socioeconomic Pathway 2-4.5 (SSP2-4.5) scenario, which assumes CO_2 emissions remain at current levels until 2050, and that there is a very likely warming range of 2.1°C to 3.5°C for 2081–2100 with respect to the 1850–1900 pre-industrial baseline [12]. The SSP2-4.5 was chosen because it represents a 'middle of the road' emissions scenario, providing an intermediate reference.

Annual mean data for `pr` from 1850 to 2100 was considered from four models to align with `tas` sources: CanESM5, IPSL-CM6A, MIROC6, and NorESM2-LM. Except for IPSL-CM6A which only provided data for a historical aerosol forcing run, historical and future data using SSP2-4.5 for `pr` was obtained from the remaining three models. The same time period of 1850–1900 was taken as the baseline for investigating `tas` and `pr` anomalies.

CMIP6 further provided data for the annual mean AOD (550nm) itemised into aerosol type from 1850–2025 for sea salt, organic aerosols, black carbon, dust, and sulfates. Historical AOD annual means (1850–2014) were computed as a multi-model mean constructed from 14 models. Projected AOD (2015–2025) similarly assumes SSP2-4.5 and is a multi-model mean constructed from five models (See Appendix F).

3 Results and Discussion

3.1 Analysis of AOD and DOD

A decline in AOD was observed in Figure 1 following 1980 for Europe and the Mediterranean, driven primarily by the reduction in sulfate aerosols. Sulfate aerosols are a component of anthropogenic emissions, being a byproduct of industrial processes and energy production, with sulfate loading peaking in the late 1970s before falling to around 40% of their maximum levels in Europe in 2014. This is largely due to the introduction of international conventions aiming to reduce emissions, such as the Convention on Long-Range Transboundary Air Pollution (CLRTAP) enforced from 1983 [13], which set pollutant reduction targets in Europe and North America. Another factor in sulfate reduction is the utilisation of abatement technologies like flue gas desulphurisation facilitating the removal of SO_2 from industrial exhaust gases.

Part of the decrease in AOD from 2015 on-

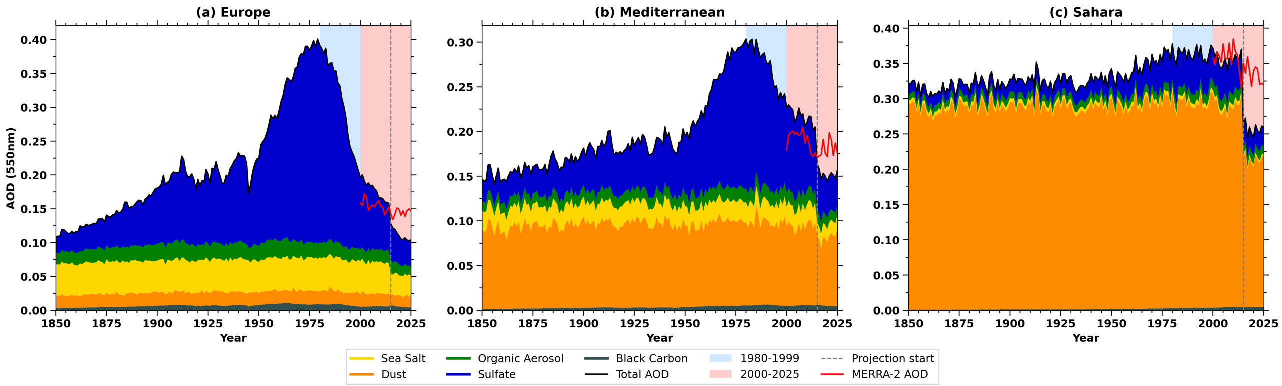

Figure 1: Time series of CMIP6 Multi-Model annual mean AOD at 550nm decomposed into aerosol type: sea salt, organic aerosol, black carbon, dust, and sulfate for 1850–2025, and MERRA-2 annual mean AOD at 550nm for 2000–2025 across regions **(a)** Europe, **(b)** Mediterranean, **(c)** Sahara from 1850–2025. Historical model runs span 1850–2014.

wards reflects an absence of a future emissions inventory for specific aerosol types in the various models under CMIP6 – for example, sea salt in Europe and dust for the Mediterranean and Sahara – rather than signifying a physically meaningful reduction in overall aerosol loading. This further explains the divergence with MERRA-2 AOD (in red).

The proportion of dust contribution to AOD rose across all three regions mainly as a result of the decrease in AOD (Table 3; see also Figure A2). This decrease was also juxtaposed against a slight increase in DOD values across all three regions.

	1980–1999		**2000–2025**	
	AOD	DOD	AOD	DOD
Europe	0.230	0.018	0.151	0.022
% of AOD		*7.9%*		*14.3%*
Mediterranean	0.233	0.084	0.188	0.086
% of AOD		*35.9%*		*45.9%*
Sahara	0.370	0.285	0.351	0.295
% of AOD		*77.0%*		*84.1%*

Table 3: MERRA-2 AOD and DOD means, and DOD proportion (%) over three regions (Europe, the Mediterranean, and the Sahara) and two periods (1980–1999 and 2000–2025)

The increase in absolute DOD values across the two periods was substantially lower for the Mediterranean and the Sahara (2.4% and 3.5% respectively) compared to a 22.2% increase for Europe. This observation of relatively steady DOD levels over the Mediterranean accompanied by stronger dust loading over Europe could suggest that dust intrusions previously constrained to the Mediterranean are extending further into the continent.

AOD and DOD displayed strong seasonality in Figure 2, showing that values were the highest in spring and summer. April and May in particular are peak months for anthropogenic emissions, exhibited by a persistent high-emission region displayed in red from 1980–1999 above central and northern Europe (40°N - 60°N). This signal is absent in the 2000–2025 period, further demonstrating a decadal improvement in air quality. Dust transport events display a similar seasonality with dust intrusions being more common between March and June, shown by the greater latitudinal reach of elevated DOD.

The seasonality of dust transport is clearly visualised in Figure 3, with spring (MAM) being the dominant season for poleward dust transport. The higher DOD values stretching over the Mediterranean and into Europe in spring signify the presence of a dust plume originating in the Sahara which is absent in other seasons. This plume was concentrated between the altitude bounds of 700 hPa and 400 hPa (roughly 3–7km), suggesting that cross-continental dust transport stays within the mid-troposphere whereas Saharan dust loading is concentrated in the lower troposphere below 700 hPa. In spring, elevated DOD extended into the Arctic and Scandinavia at higher latitudes between 600–300 hPa, reaching the top of the mid-troposphere. In summer, whilst dust loading in the Sahara was less pronounced than spring and further removed from the surface, the vertical reach of DOD remained high. Over Europe, DOD was restricted to a narrower vertical range in summer than in spring, with most of the dust loading being concentrated between 700–500 hPa. The remaining seasons (winter and autumn) saw DOD confined to lower altitudes, reaching a maximum of 400 hPa.

The primary Saharan dust sources are in Algeria, Libya, and Niger. Figure 4 further con-

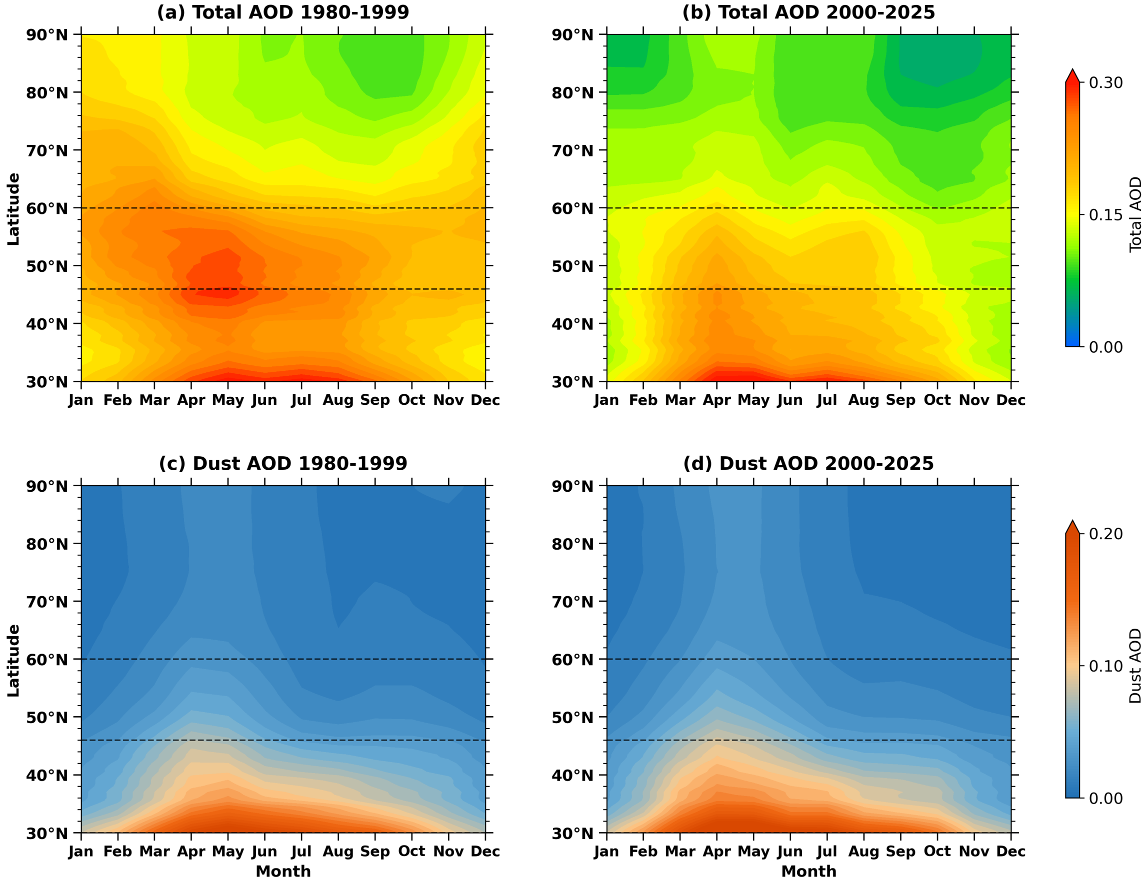

Figure 2: Monthly zonal MERRA-2 averages for January to December from 30°N to 90°N of **(a)** Total AOD 1980–1999, **(b)** Total AOD 2000–2025, **(c)** Dust AOD 1980–1999, **(d)** Dust AOD 2000–2025. Black dotted lines at 46°N and 60°N indicate the upper boundaries of the Mediterranean and Europe respectively.

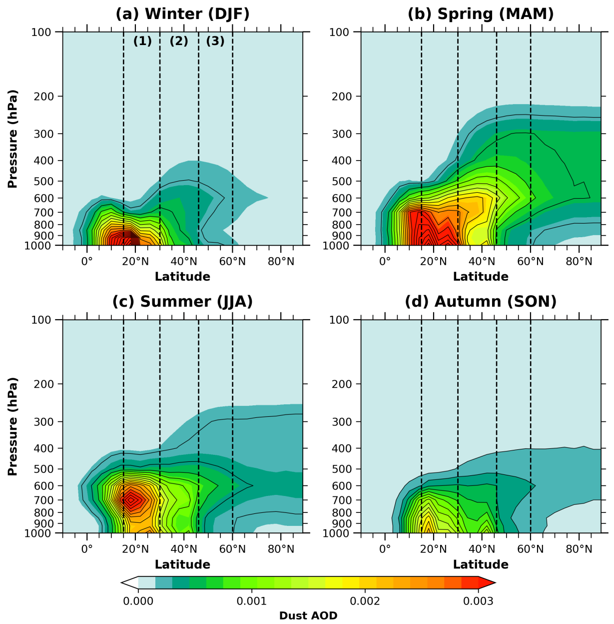

Figure 3: Seasonal zonal mean vertical profiles of GEOS-Chem DOD (550nm) from 2003–2012 for **(a)** Winter (DJF), **(b)** Spring (MAM), **(c)** Summer (JJA), and **(d)** Autumn (SON). Atmospheric pressure (hPa) from 1000–100 hPa by latitude from 10°S to 90°N. Regions (1), (2), and (3) in dashed lines are the latitudinal bounds of the Sahara, the Mediterranean, and Europe.

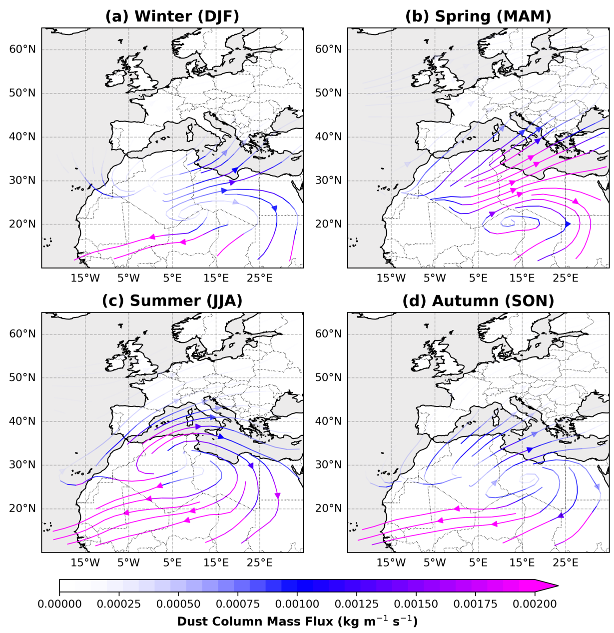

Figure 4: Seasonal means of MERRA-2 DUFLUXU and DUFLUXV from 1980–2025 over the Sahara, the Mediterranean, and Europe for **(a)** Winter (DJF), **(b)** Spring (MAM), **(c)** Summer (JJA), **(d)** Autumn (SON). Streamlines and arrows indicate the direction of flux. Colour shading indicates magnitude of mass flux (kg m^{-1} s^{-1}).

firms that spring is the dominant season for dust transport, seen both in the path of dust column mass flux vectors to Europe and the magnitude of the transport vector. Spring and summer are the most active months for dust lifting from the Sahara seen in the density of streamlines; however, the direction of streamlines in summer indicates that westward transport is more prevalent over the Atlantic Ocean compared to northward movement. In fact, spring showed the least trans-Atlantic dust mass flux; this could suggest that the high springtime DOD over Europe is the result of a seasonal shift in the dominating transport pathway.

3.2 Dust Events

3.2.1 Event Characteristics

From 1980–2025, there were a total of 284 dust events identified in Europe. 16,742 days were considered, of which there were 1,900 dust days (11.3%) where $\overline{\text{DOD}}(d) \leq \text{DOD}_{\text{clim}} + \sigma$. The seasonal and categorical breakdown of the dust events can be seen in Table 4, with an average of 1.6 events per season each year. Winter exhibited the highest number of extreme dust events, which were driven primarily by February events and a lower winter threshold. Although dust transport to Europe occurs predominantly in spring and summer, using seasonal thresholds results in a higher DOD_{clim} and σ during peak dust-loading seasons, thereby raising the statistical threshold values for an extreme event. Consequently, notable events during spring may be classified as strong rather than extreme.

Season	Moderate	Strong	Extreme
DJF	31	31	8
MAM	33	36	2
JJA	45	24	3
SON	37	31	3
Total	146	122	16

Table 4: Number of identified dust events by category and season from 1980–2025 based on MERRA-2 threshold methodology.

Figure 5 shows the characteristics of identified dust events in Europe for selected months. February exhibited a clear succession of extreme events from 2020 onwards, suggesting that the intensity of dust events has increased leading into spring in the last five years. March also showed an extreme event in 2024 following the succession of four strong dust events from 2020 onwards. There appears to be no clear change in the frequency of dust events for the selected months, although events in March seem to occur in clusters, particularly in the 2003–2009 and 2020–2025 periods.

The observed change in event intensity for February was supported by Mann-Whitney U tests applied to two sample groups, which showed that based on a 2020–2025 sample group compared to 1980–2019, February demonstrated a statistically significant increase in DOD_{avg}. Based on these two sample groups, no months showed a statistically significant increase in event duration, but March and June showed a statistically significant increase in event frequency. Whilst no other months were identified as having higher event intensity, Europe showed a statistically significant increase in event intensity in 2020–2025 compared to 1980–2019 according to t-test results in Table 5. Monthly findings should be caveated by a small sample size n for dust event data in the 2020–2025 period, where $0 \leq n \leq 11$. Therefore, the data subset may be too small to draw conclusions about long-term changes in dust event patterns.

	Gaussian		Log-Normal	
	t	***p***	***t***	***p***
DOD_{avg}	-2.731	0.007	-2.661	0.008
Duration	-0.181	0.856	-0.651	0.515
Frequency	0.031	0.975	–	–

Table 5: T-tests comparing dust event intensity (DOD_{avg}), duration (days), and frequency (number of events per month) for 1980–2019 and 2020–2025, under Gaussian and log-normal distributions.

Based on t-tests applied to two sample groups of 1980–1999 and 2000–2025, it was found that Europe did not show a statistically significant change in intensity or frequency of dust events (Table 6). The duration of events showed a statistically significant increase, suggesting that on a multi-decadal time frame, instances of anomalous dust loading over Europe have become more prolonged. This trend was reinforced for June and September through the Mann-Whitney U tests, which confirmed that these months showed an increase in event duration. June showed an increase in frequency whereas no months showed an increase in event intensity between 1980–1999 and 2000–2025 . See Appendix D and E for full μ and p values.

3.2.2 AERONET Comparison

From a sample size of 107,923 data points from 121 sites in Europe, MERRA-2 daily AOD

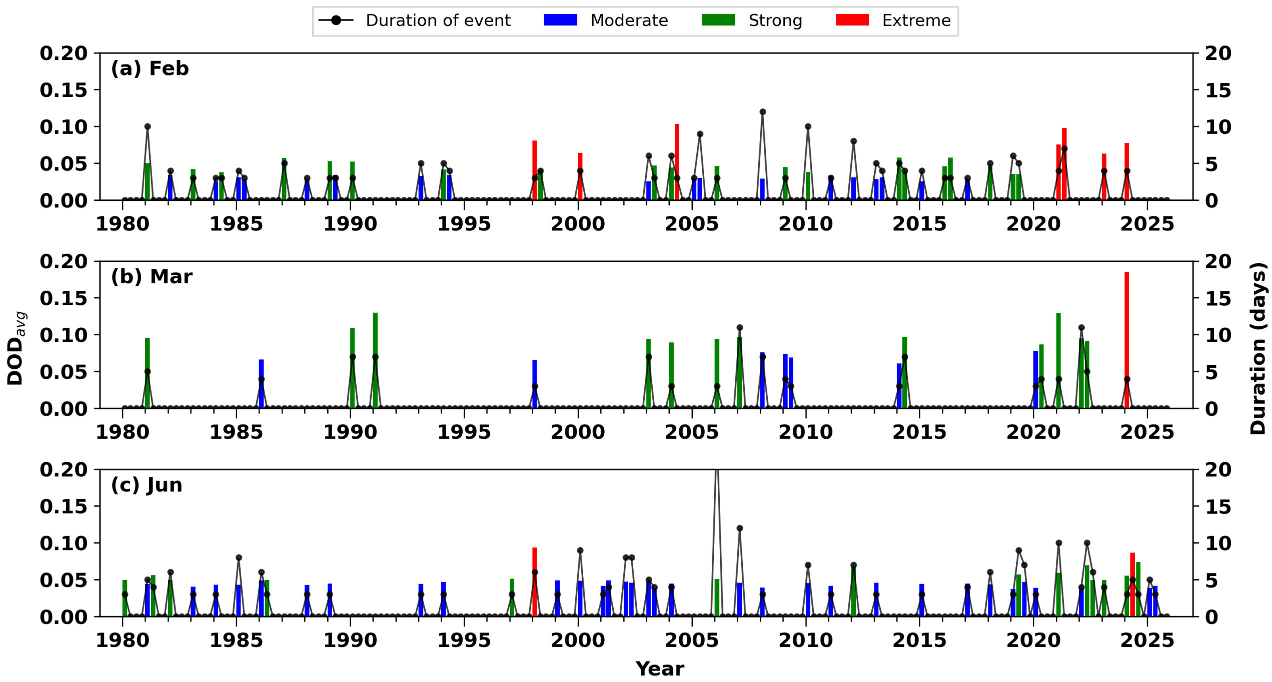

Figure 5: Monthly time series (1980–2025) for occurrence of European dust events showing event intensity (DOD_{avg}, left y axis) and event duration in days (black dots and lines, right y axis) for **(a)** February, **(b)** March, and **(c)** June. Bar colours indicate the dust event category: blue for moderate, green for strong, and red for extreme. Outlier dust event in June 2006 lasted 26 days.

	Gaussian		Log-Normal	
	t	p	t	p
DOD_{avg}	-1.133	0.258	-1.062	0.289
Duration	-3.146	0.002	-3.139	0.002
Frequency	-0.600	0.549	–	–

Table 6: T-tests comparing dust event intensity (DOD_{avg}), duration (days), and frequency (number of events per month) for 1980–1999 and 2000–2025, under Gaussian and log-normal distributions.

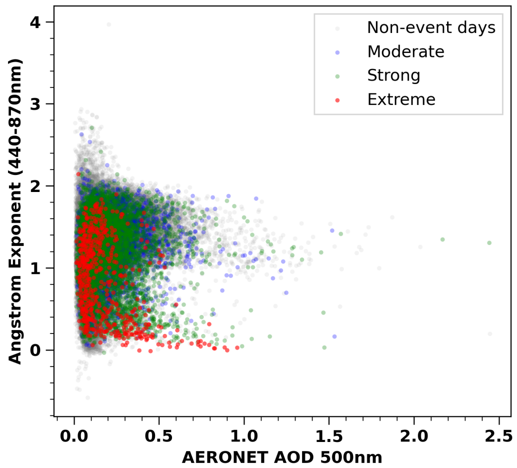

Figure 6: Scatter plots for AERONET daily Angstrom exponent (440-870nm) against daily AOD at 500nm for sites located in Europe (121 sites) for 1980–2025. Point colours correspond to the category of dust event the plotted day falls under: grey (no event), blue (moderate event), green (strong event), and red (extreme event).

(550nm) compared to AERONET daily AOD (500nm) had moderate correlation of $r = 0.435$ and a bias of -0.002. RMSE was 0.108, signalling a proportionally high uncertainty considering mean AERONET daily AOD was 0.201 during event days, and 0.154 during non-event days. This error could indicate a limitation of the dust event categorisation applied; it lacks the spatial granularity for identifying dust events over individual AERONET sites as DOD thresholds are based on a spatial average, disguising city or country-specific signals. In general, using spatial averages over Europe to identify dust events smooths out local extremes, whereas validation data uses point measurements which do capture such extremes. This may be a contributing factor in the moderate MERRA-2 and AERONET agreement.

The dust categorisation methodology showed some agreement with AERONET data in the identification of extreme events, seen in the pull of red points into the $0 \leq \alpha \leq 0.5$ and high AOD section in Figure 6. From this, it can be inferred that for some extreme events based on MERRA-2 thresholds, AERONET measurements agree that coarse aerosols like dust and sea salt are dominant contributors to AOD. Distinctions between

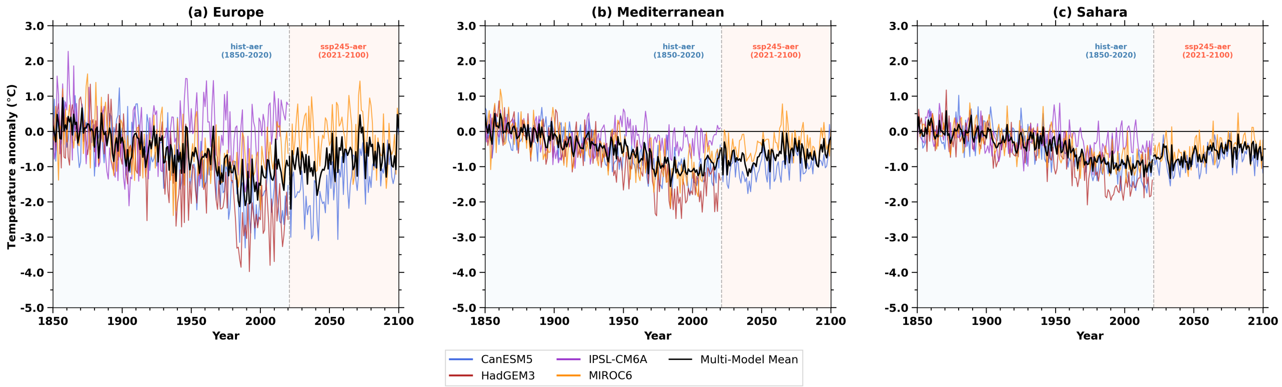

Figure 7: Time series of CMIP6 Near-Surface Air Temperature anomaly (°C) from 1850–2100 for **(a)** Europe, **(b)** the Mediterranean, and **(c)** the Sahara as a result of aerosol-only forcing using an 1850–1900 pre-industrial mean as the baseline. Historical runs (hist-aer, 1850–2020) and future runs (ssp245-aer, 2021–2100) shown for four models, with future runs assuming SSP2-4.5. The multi-model mean is computed from these models.

moderate and strong events were less evident, with most blue and green points clustered in $1 \leq \alpha \leq 2$. This could be attributed to relatively higher urban pollution contributions to AOD on days with lower dust loading.

3.3 Climate Variables

Investigating the effects of total aerosol forcing on temperature shows a reversal of the aerosol cooling effect following 2000 in Figure 7. Total aerosol forcing was found to have produced a historic net cooling effect on near-surface air temperatures across Europe, the Mediterranean, and the Sahara through aerosol scattering and absorption of incoming sunlight, shown in the negative temperature anomaly gradients. Projections show that total aerosol forcing is becoming a positive driver of temperatures from 2000–2100 under an SSP2-4.5 scenario, contributing to rising regional temperatures. Model outputs show that temperature will rise above the 1850–1900 baseline in Europe by 2100, with Europe also showing the clearest trend reversal out of the three considered regions. This is consistent with the observed trend of declining AOD, where the initial warming effect could be attributed to reduced extinction of incoming solar radiation. Aerosol forcing showed no effect on precipitation, with anomalies remaining level from 1850–2100 for all three regions (see Appendix G).

Due to the model showing temperature change resulting from total aerosol forcing rather than decomposition into forcing by aerosol type, investigating the effects of dust forcing on temperature did not yield conclusive results. The relationship between the increasing intensity of dust events and the modelled warming effect remains unclear as further information is required to determine whether the climate models capture the increasing intensity of dust events from 2020–2025 in future runs. This is an opportunity for expanding on the report's research.

4 Conclusion

This report has investigated the shifts in dust event patterns from 1980–2025, examining changes in event characteristics and contrast with AOD trends for Europe. Dust events have been identified and categorised based on MERRA-2 DOD seasonal thresholds. The central conclusions are as follows.

1. The decrease in AOD is driven primarily by a reduction in sulfates from anthropogenic emissions. This decrease is concurrent with a slight increase in DOD, with Europe showing the greatest relative increase. Comparing 1980–1999 with 2000–2025 period means shows these changes are especially pronounced in spring and summer (Mar–Aug), consistent with Saharan dust transport peaking during spring and summer.

2. For the three characteristics considered of dust transport events, generally the intensity and duration of events are changing whereas frequency remains consistent from 1980 to 2025. Changes in event characteristics depend on sample group selection; based on t-tests for 1980–1999 compared to 2000–2025, there was a statistically significant increase in European event duration. For 1980–2019 compared to 2020–2025, t-tests showed a statistically significant increase in event intensity.

3. Comparisons between 1980–1999 and 2000–2025 showed that event duration increased in June and September, event frequency increased in June, and event intensity increased in no

months. For 1980–2019 and 2020–2025, event duration increased in no months, event frequency increased in March and June, and event intensity increased in February.

4. Following 2000, total aerosol forcing has a warming effect on near-surface air temperature compared to a historic cooling effect. This further underscores the importance of understanding changes in AOD for climate change.

Further research is required to address the relationship between changes in dust event characteristics and regional warming through isolating the radiative forcing effects from dust aerosols. Future work could refine the spatial granularity of the threshold-based methodology by narrowing the coordinate ranges for DOD_{clim} and σ to improve identification of local extreme events. As the catalogue of 2020–2025 dust events extends beyond 2025, repeating the statistical tests will determine whether recent dust event trends are sustained or episodic.

References

[1] Food Department for Environment and Rural Affairs. *Air quality statistics in the UK, 1987 to 2024 - Particulate matter (PM10/PM2.5)*. 2025. URL: https://www.gov.uk/government/statistics/air-quality-statistics/concentrations-of-particulate-matter-pm10-and-pm25 (visited on 2026-02-25).

[2] S. Y. Kyung and S. H. Jeong. "Particulate-Matter Related Respiratory Diseases". In: *Tuberculosis and Respiratory Diseases* 83.2 (2020), pp. 116–121. DOI: 10.4046/trd.2019.0025.

[3] O. Bamisile et al. "The environmental factors affecting solar photovoltaic output". In: *Renewable and Sustainable Energy Reviews* 208 (2025), p. 115073. ISSN: 1364-0321. DOI: https://doi.org/10.1016/j.rser.2024.115073. URL: https://www.sciencedirect.com/science/article/pii/S1364032124007998.

[4] UN. General Assembly (78th sess. : 2023-2024). *United Nations Decade on Combating Sand and Dust Storms (2025-2034) : resolution / adopted by the General Assembly*. 2024. URL: https://digitallibrary.un.org/record/4054463?v=pdf (visited on 2026-02-25).

[5] United Nations. *Sand and Dust Storms Coalition*. URL: https://www.unccd.int/land-and-life/sand-dust-storm/overview (visited on 2026-04-25).

[6] M. G. Bosilovich et al. *MERRA-2: Initial Evaluation of the Climate*. Technical Report Series on Global Modeling and Data Assimilation. National Aeronautics and Space Administration, 2015.

[7] Global Modeling and Assimilation Office (GMAO). *MERRA-2* $tavg1_2d_aer_Nx$: $2d, 1 - Hourly, Time - averaged, Single - Level, Assimilation, AerosolDiagnosticsV$ 5.12.4. Greenbelt, MD, USA, 2015. DOI: 10.5067/KLICLTZ8EM9D. (Visited on 2025-12-03).

[8] A. Gkikas et al. "Mediterranean intense desert dust outbreaks and their vertical structure based on remote sensing data". In: *Atmospheric Chemistry and Physics* 16.13 (2016), pp. 8609–8642. DOI: 10.5194/acp-16-8609-2016. URL: https://acp.copernicus.org/articles/16/8609/2016/.

[9] E. Cuevas-Agulló et al. "Sharp increase in Saharan dust intrusions over the western Euro-Mediterranean in February–March 2020–2022 and associated atmospheric circulation". In: *Atmospheric Chemistry and Physics* 24.7 (2024), pp. 4083–4104. DOI: 10.5194/acp-24-4083-2024. URL: https://acp.copernicus.org/articles/24/4083/2024/.

[10] I. Bey et al. "Global modeling of tropospheric chemistry with assimilated meteorology: Model description and evaluation". In: *Journal of Geophysical Research: Atmospheres* 106.D19 (2001), pp. 23073–23095. DOI: https://doi.org/10.1029/2001JD000807. URL: https://agupubs.onlinelibrary.wiley.com/doi/abs/10.1029/2001JD000807.

[11] B.N. Holben et al. "AERONET—A Federated Instrument Network and Data Archive for Aerosol Characterization". In: *Remote Sensing of Environment* 66.1 (1998). [https://aeronet.gsfc.nasa.gov], pp. 1–16. ISSN: 0034-4257. DOI: 10.1016/S0034-4257(98)00031-5. URL: https://www.sciencedirect.com/science/article/pii/S0034425798000315.

[12] IPCC. *Climate Change 2023: Synthesis Report. Contribution of Working Groups I, II and III to the Sixth Assessment Report of the Intergovernmental Panel on Climate Change*. Ed. by H. Lee and J. Romero. [Core Writing Team, H. Lee J. Romero (eds.)] Geneva, Switzerland, 2023. DOI: 10.59327/IPCC/AR6-9789291691647.

[13] United Nations. *1979 Convention on Long-Range Transboundary Air Pollution*. 1979. URL: https://treaties.un.org/pages/ViewDetails.aspx?src=TREATY&mtdsg_no=XXVII-1&chapter=27&clang=_en (visited on 2026-03-22).

A Monthly MERRA-2 AOD and DOD

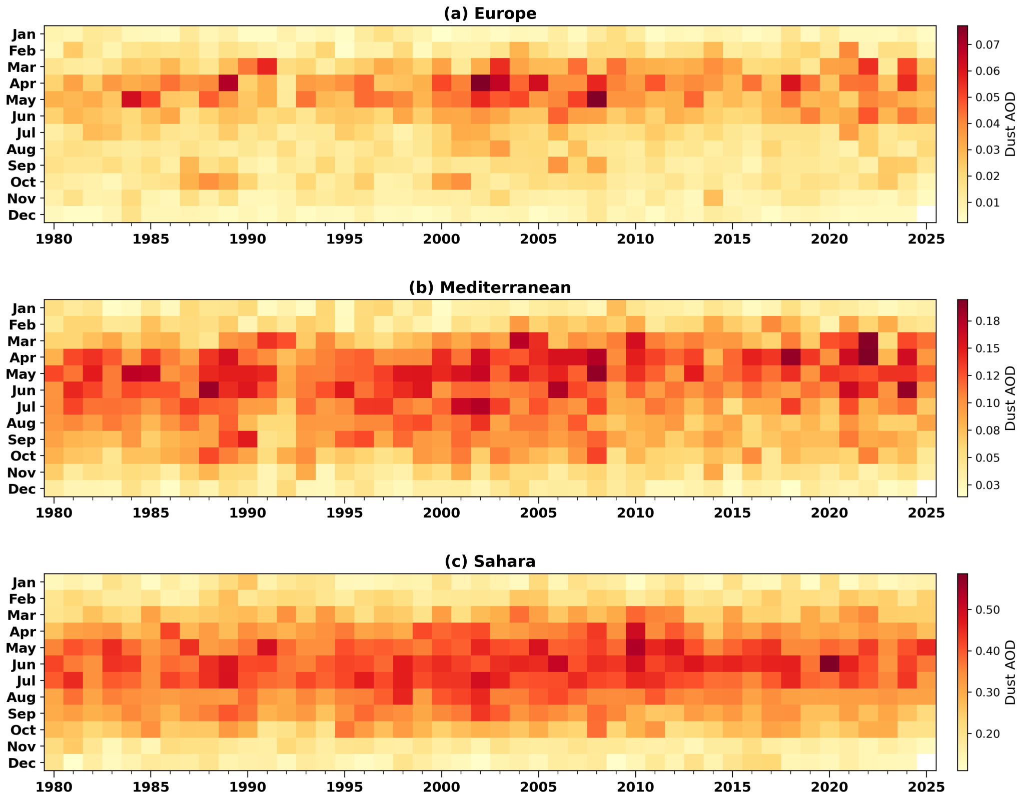

Figure A1: Colour matrix of MERRA-2 DOD monthly averages for **(a)** Europe, **(b)** the Mediterranean, and **(c)** the Sahara from 1980–2025.

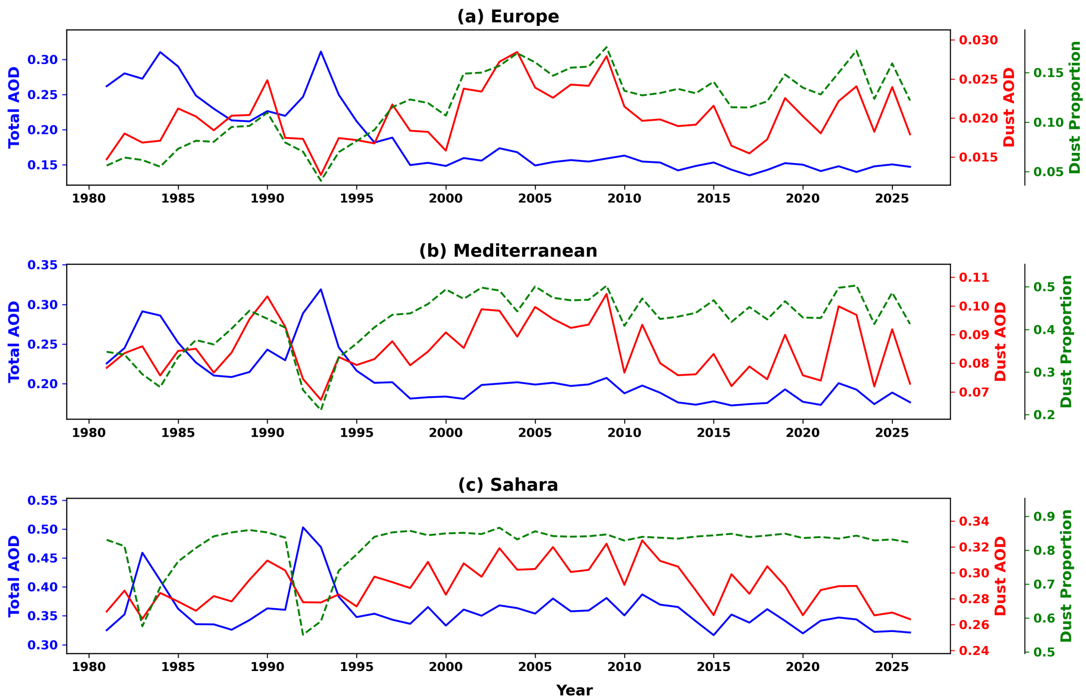

Figure A2: Time series of average monthly MERRA-2 AOD, average monthly MERRA-2 DOD, and Dust Proportion (DOD as a fraction of AOD) from 1980–2025 in three regions: **(a)** Europe, **(b)** the Mediterranean, and **(c)** the Sahara.

B AERONET Locations

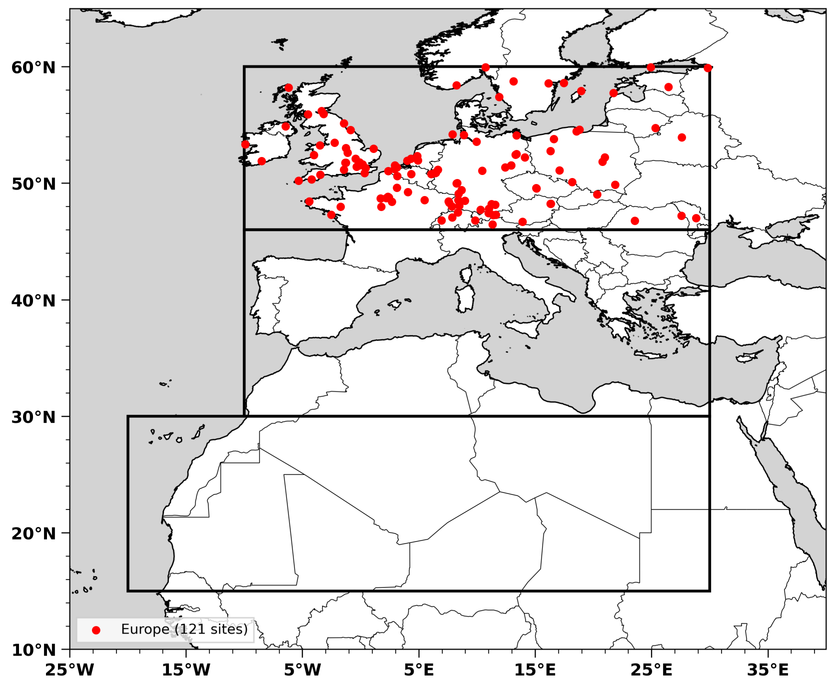

Figure B1: Map showing regions in black boxes: Europe (10°W, 30°E, 46°N, 60°N), the Mediterranean (10°W, 30°E, 30°N, 46°N), the Sahara (20°W, 30°E, 15°N, 30°N) with 121 considered AERONET sites in Europe shown in red dots.

C Gaussian and Log-Normal Fittings

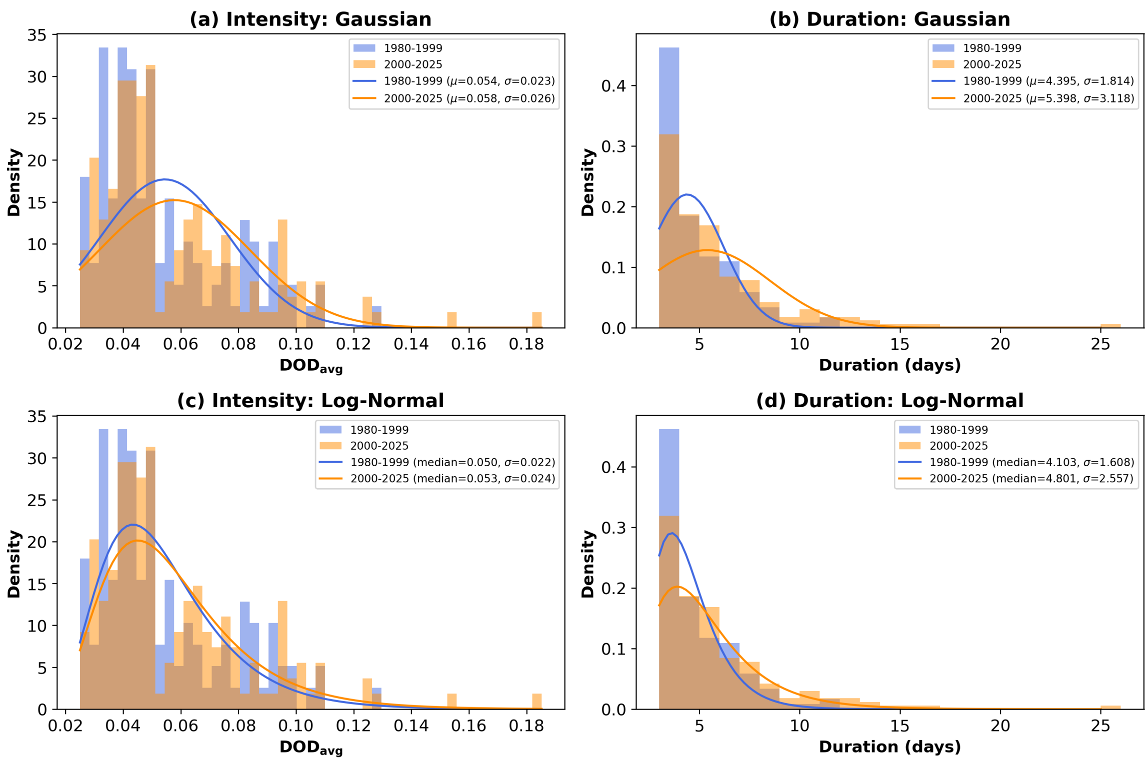

Figure C1: Distribution of European dust event intensity (DOD_{avg}) (left) and dust event duration (days) (right) across two periods: 1980–1999 (blue) and 2000–2025 (orange). Upper panels show fitted Gaussian distributions with mean (μ) and standard deviation (σ) in the legend. Lower panels show fitted log-normal distributions, with median and σ in the legend.

D Statistical Tests (1980–1999 and 2000–2025)

Europe – frequency			
Month	**μ (1980–1999)**	**μ (2000–2025)**	**p**
Jan	0.55	0.35	0.916
Feb	0.85	1.08	0.163
Mar	0.25	0.58	0.075
Apr	0.55	0.65	0.184
May	0.55	0.50	0.673
Jun*	0.80	1.23	0.046
Jul	0.35	0.35	0.495
Aug	0.10	0.23	0.129
Sep	0.70	0.50	0.811
Oct	0.70	0.46	0.881
Nov	0.40	0.38	0.763
Dec	0.15	0.08	0.789

Table D1: Mann-Whitney tests for Europe – average number of dust events per year μ and p-value by month (Sample size $n = 20$ for 1980–1999, $n = 26$ for 2000–2025). * signifies month with statistically significant changes.

Europe – duration			
Month	**μ (1980–1999)**	**μ (2000–2025)**	**p**
Jan	4.182	4.333	0.452
Feb	4.000	4.964	0.052
Mar	5.200	5.267	0.674
Apr	4.455	6.353	0.235
May	5.091	5.692	0.306
Jun*	4.062	6.031	0.020
Jul	4.143	4.333	0.345
Aug	3.000	5.500	0.060
Sep*	4.286	6.462	0.019
Oct	4.786	5.167	0.243
Nov	5.000	4.000	0.935
Dec	3.667	3.000	0.952

Table D2: Mann-Whitney tests for Europe – average duration (days) of dust events μ and p-value by month (Sample size ranges from $n = 2$ to 17 for 1980–1999, $n = 2$ to 32 for 2000–2025). * signifies month with statistically significant changes.

Europe – intensity			
Month	**μ (1980–1999)**	**μ (2000–2025)**	**p**
Jan	0.040	0.037	0.676
Feb	0.041	0.047	0.275
Mar	0.093	0.094	0.600
Apr	0.090	0.097	0.240
May	0.080	0.074	0.888
Jun	0.050	0.049	0.681
Jul	0.055	0.051	0.697
Aug	0.048	0.051	0.571
Sep	0.041	0.039	0.660
Oct	0.053	0.050	0.631
Nov	0.042	0.040	0.770
Dec	0.027	0.038	0.100

Table D3: Mann-Whitney tests for Europe – average intensity (DOD_{avg}) of dust events μ and p-value by month (Sample size ranges from $n = 2$ to 17 for 1980–1999, $n = 2$ to 32 for 2000–2025). * signifies month with statistically significant changes.

E Statistical Tests (1980–2019 and 2020–2025)

Europe – frequency			
Month	**μ (1980–2019)**	**μ (2020–2025)**	**p**
Jan	0.45	0.33	0.709
Feb	1.02	0.67	0.860
Mar*	0.35	1.00	0.023
Apr	0.65	0.33	0.804
May	0.55	0.33	0.695
Jun*	0.93	1.83	0.012
Jul	0.35	0.33	0.476
Aug	0.15	0.33	0.143
Sep	0.57	0.67	0.385
Oct	0.60	0.33	0.795
Nov	0.45	0.00	0.965
Dec	0.12	0.00	0.826

Table E1: Mann-Whitney tests for Europe – average number of dust events per year μ and p-value by month (Sample size $n = 40$ for 1980–2019, $n = 6$ for 2020–2025). * signifies month with statistically significant changes.

Europe – duration			
Month	**μ (1980–2019)**	**μ (2020–2025)**	**p**
Jan	4.222	4.500	0.447
Feb	4.585	4.750	0.208
Mar	5.286	5.167	0.534
Apr	5.692	4.500	0.590
May	5.636	3.000	0.962
Jun	5.459	5.091	0.459
Jul	4.000	6.000	0.099
Aug	5.000	4.500	0.302
Sep	5.261	5.750	0.163
Oct	4.833	6.500	0.114
Nov	4.444	–	–
Dec	3.400	–	–

Table E2: Mann-Whitney tests for Europe – average duration (days) of dust events μ and p-value by month (Sample size ranges from $n = 5$ to 41 for 1980–2019, $n = 0$ to 11 for 2020–2025). – indicates no events recorded in that period. * signifies month with statistically significant changes.

Europe – intensity			
Month	**μ (1980–2019)**	**μ (2020–2025)**	**p**
Jan	0.038	0.047	0.132
Feb*	0.041	0.078	0.000
Mar	0.087	0.111	0.156
Apr	0.094	0.096	0.519
May	0.077	0.074	0.562
Jun	0.048	0.055	0.157
Jul	0.052	0.059	0.350
Aug	0.051	0.048	0.571
Sep	0.040	0.039	0.616
Oct	0.053	0.042	0.828
Nov	0.041	–	–
Dec	0.031	–	–

Table E3: Mann-Whitney tests for Europe – average intensity (DOD_{avg}) of dust events μ and p-value by month (Sample size ranges from $n = 5$ to 41 for 1980–2019, $n = 0$ to 11 for 2020–2025). – indicates no events recorded in that period. * signifies month with statistically significant changes.

F CMIP6 Models

No.	Model Name	Modelling Centre / Institute ID, Country	Resolution (Lat x Lon)	Aerosol Scheme	Period
1	CESM2-WACCM-FV2	National Center for Atmospheric Research, USA	1.9° × 2.5°	Modal Aerosol Module (MAM4)	H
2	CNRM-ESM2-1	Centre National de Recherches Meteorologiques, France	1.4° × 1.4°	Tropospheric Aerosols for ClimaTe In CNRM (TACTICv2)	H+F
3	EC-Earth3-AerChem	Swedish Meteorological and Hydrological Institute, Sweden	2° × 3°	Chemistry transport model (TM5)	H
4	GISS-E2-1-G	Goddard Institute for Space Studies, USA	2.0° × 2.5°	One-Moment Aerosol scheme (OMA)	H
5	GISS-E2-1-H	Goddard Institute for Space Studies, USA	2.0° × 2.5°	One-Moment Aerosol scheme (OMA)	H
6	INM-CM4-8	Institute for Numerical Mathematics, Russia	1.5° × 2.0°	INM-AER1	H+F
7	INM-CM5-0	Institute for Numerical Mathematics, Russia	1.5° × 2.0°	INM-AER1	H
8	IPSL-CM5A2-INCA	Institut Pierre Simon Laplace, France	2.00° × 3.75°	none	H
9	IPSL-CM6A-LR-INCA	Institut Pierre Simon Laplace, France	1.26° × 2.5°	INteraction with Chemistry and Aerosols module (INCA v6 AER)	H
10	MIROC6	Japan Agency for Marine-Earth Science and Technology, Japan	2.8° × 2.8°	SPectral RadIatioN-TrAnSport module (SPRINTARS6.0)	H+F
11	MPI-ESM-1-2-HAM	Max Planck Institut fur Meteorologie, Germany	1.875° × 1.875°	Hamburg Aerosol Module version 2.3 (HAM2.3)	H
12	MRI-ESM2-0	Meteorological Research Institute, Japan	1.125° × 1.125°	Model of Aerosol Species IN the Global AtmospheRe (MASINGAR mk2r4)	H+F
13	NorESM2-LM	Meteorological Institute, Norway	2.5° × 1.875°	Oslo aerosol module (OsloAero)	H+F
14	NorESM2-MM	Meteorological Institute, Norway	1.00° × 1.25°	Oslo aerosol module (OsloAero)	H

Table F1: CMIP6 models used in the study of AOD evolution and composition. H signifies use of historical model run only (1850–2014); H+F signifies use of historical run and SSP-2.45 future projections (2015–2025).

G CMIP6 Precipitation Anomaly

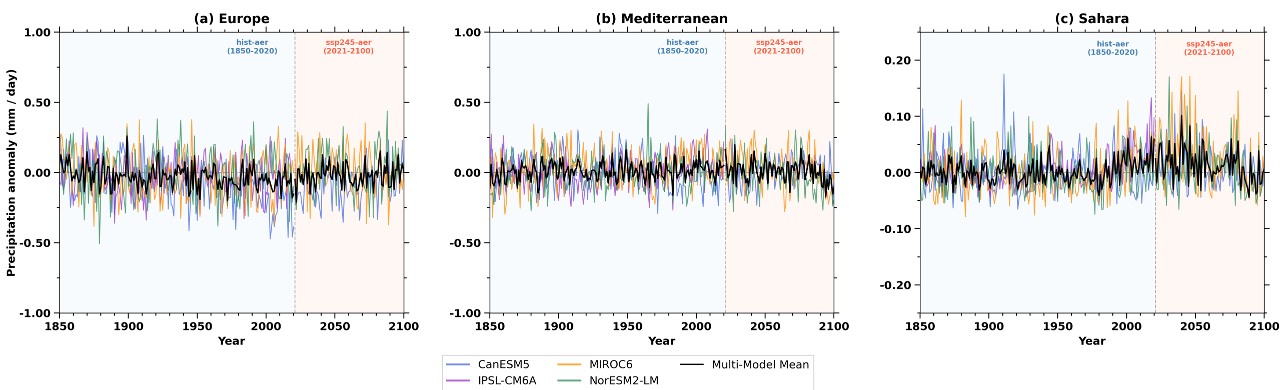

Figure G1: Time series of CMIP6 Precipitation anomaly (mm / day) from 1850–2100 for **(a)** Europe, **(b)** the Mediterranean, and **(c)** the Sahara as a result of aerosol-only forcing using an 1850–1900 pre-industrial mean as the baseline. Historical runs (hist-aer, 1850–2020) and future runs (ssp245-aer, 2021–2100) shown for four models, with future runs assuming SSP2-4.5. The multi-model mean is computed from these models.